Russian Journal *of* Earth Sciences Online ISSN: 1681-1208

Special Issue: "Kamchatka Earthquake M 8.8 on July 29, 2025"

Analysis of Ionospheric Parameter Dynamics During a Strong Earthquake in Kamchatka on July 29, 2025, Based on a Complex Approach (According to the Data of Ionosphere Vertical Radio Sounding and GNSS)

A. V. Pavlov[*,1], **O. V. Mandrikova**[1], **and N. N. Titkov**[2]

[1]Institute of Cosmophysical Research and Radio Wave Propagation FEB RAS, Paratunka, Russian Federation
[2]Kamchatka Branch of the Federal Research Center "Geophysical Survey of RAS", Petropavlovsk-Kamchatskiy, Russian Federation

* **Correspondence to:** Aleksey Pavlov, pavlov@ikir.ru

Abstract: Using a complex of tools for data recording and analysis, the paper investigates ionospheric parameter dynamics during a strong earthquake in Kamchatka on July 29, 2025 (magnitude $M = 8.8$). The data of the ionospheric critical frequency f_oF_2 of Paratunka observatory (Kamchatka, IKIR FEB RAS), and the data of the regional GNSS receiver network, located near the earthquake source, were under analysis. Using data from GNSS receivers, the values of absolute vertical total electron content (TEC) and disturbance indices of vertical TEC variations (WTEC) were studied. Data detailed analysis was realized using a new method based on wavelet transform. For the estimates, anomaly intensity measure, characterizing weak, moderate and strong ionospheric disturbances, was used. Before and during the earthquake on July 29, 2025, anomalous changes were distinguished in ionospheric parameter time series. They characterize moderate and intensive oscillation processes in the ionosphere exceeding the background level. A large-scale long (about 2 days) negative anomaly was detected three days and a half before the earthquake against the background of low geomagnetic activity according to the data of Paratunka observatory and GNSS receivers. During the development of the aftershock process, according to data from the Paratunka observatory and data from all GNSS receivers, a large-scale positive anomaly was identified, exceeding in intensity the background variations in ionospheric parameters by three times and more. The positive anomaly lasted for about 2 days. In the region of PAUJ station, the ionospheric disturbances were the most intensive and significantly exceeded in amplitude the disturbances, observed during the period under analysis when geomagnetic activity increased.

Keywords: Seismic activity, seismo-ionospheric coupling, total electron content, ionospheric disturbances, wavelet transform, Kamchatka megathrust earthquake

Citation: Pavlov A. V., Mandrikova O. V., and Titkov N. N. (2026), Analysis of Ionospheric Parameter Dynamics during a Strong Earthquake in Kamchatka on July 29, 2025, Based on a Complex Approach (According to the Data of Ionosphere Vertical Radio Sounding and GNSS), *Russian Journal of Earth Sciences*, 26, ES2019, EDN: TCBKCK, https://doi.org/10.2205/2026es001129

Research Article

Received: February 2, 2026
Accepted: May 25, 2026
Published: July 1, 2026

1. Introduction

Using a complex of tools for data recording and analysis, the paper investigates ionospheric parameter dynamics during a very strong earthquake near the eastern coast of Kamchatka peninsula (at 23:24:53 UT on July 29, 2025) with the magnitude $M = 8.8$. It was illustrated in a number of investigations that such extreme natural events as earthquakes and volcano eruptions may initiate ionospheric disturbances and be reflected in ionospheric parameter variations near the sources of their generation [*Bogdanov and Pavlov*, 2023;

Bošková et al., 1994; *Budak et al.*, 2024; *Depueva et al.*, 2007; *Hegai et al.*, 2011; *Karatay et al.*, 2025; *Ke et al.*, 2016; *Liu and Xu*, 2016; *Maruyama et al.*, 2011; *Pulinets et al.*, 2018b; *Rodkin and Liperovskaya*, 2023; *Tachema*, 2024]. According to the results of the papers [*Bogdanov and Pavlov*, 2023; *Bošková et al.*, 1994; *Budak et al.*, 2024; *Depueva et al.*, 2007; *Hegai et al.*, 2011; *Karatay et al.*, 2025; *Ke et al.*, 2016; *Liu and Xu*, 2016; *Maruyama et al.*, 2011; *Pulinets et al.*, 2018b; *Rodkin and Liperovskaya*, 2023; *Tachema*, 2024], ionospheric anomalies may be observed before strong earthquakes and can be considered as one of possible precursors of seismic events. However, ionospheric variability and the disturbances associated with solar and geomagnetic activities [*Danilov and Konstantinova*, 2023; *Ivanov et al.*, 2011; *Perevalova et al.*, 2023, 2015; *Smirnova and Smirnov*, 2013; *Taurenis et al.*, 2022; *Zherebtsov et al.*, 2021], make it more difficult to detect and to interpret unequivocally seismic anomalies having significantly lower amplitude in most cases [*Afraimovich et al.*, 2004; *Bogdanov and Pavlov*, 2023; *Mandrikova and Fetisova*, 2026; *Rodkin and Liperovskaya*, 2023]. Thus, investigation of ionospheric processes requires a complex approach and improvement of the methods for ionospheric data recording and analysis [*Bilitza et al.*, 2022; *Goncharenko et al.*, 2021].

In recent years, data of total electron content (TEC), obtained by the navigation GNSS receiver measurements, are widely applied to investigate ionospheric processes [*Afraimovich and Perevalova*, 2006; *Hofmann-Wellenhof et al.*, 1992]. Anomalous changes in TEC were multiply observed during powerful eruptions of volcanoes both at high latitudes and near the equator [*Pulinets et al.*, 2022a; *Ryabova and Shalimov*, 2024]. In a number of papers [*Bolsunovskii et al.*, 2024; *Budak et al.*, 2024; *Karatay et al.*, 2025; *Ke et al.*, 2016; *Liu and Xu*, 2016; *Pulinets et al.*, 2015; *Tachema*, 2024; *Zakharchenkova et al.*, 2012], anomalies in TEC before strong earthquakes were observed within the interval from several hours up to several days before events. Under conditions of moderate geomagnetic activity, such anomalies can be considered as possible short-term ionospheric precursors of earthquakes and it is of scientific and applied interest to investigate them. Based on the GNSS data, the paper [*Liu and Xu*, 2016] statistically analyzes local TEC anomalies before 121 strong ($M \geq 7.0$) earthquakes. In the research [*Liu and Xu*, 2016] the moving median differential estimation method together with a new method for image processing were used. The results [*Liu and Xu*, 2016] showed that significant local anomalies in TEC data were observed up to six days before 80 earthquakes under consideration (about 66.1% from the total number). Both positive and negative anomalies of different intensity and duration were observed before the earthquakes. Positive anomalies were more frequently observed than negative ones. According to the results [*Liu and Xu*, 2016], local time distribution of TEC anomalies, observed before the earthquakes, occurred mainly during the nighttime. Moreover, most of them were not above the epicenter but shifted southward.

In another paper [*Ke et al.*, 2016] the relation between earthquakes and TEC anomalies in the ionosphere based on GNSS data was under the study. The authors considered 24 earthquakes with $5.0 < M < 8.0$, which occurred in China in 2003–2013. The investigation [*Ke et al.*, 2016] also showed the possibility of occurrences of positive and negative TEC anomalies during earthquakes. It was noticed [*Ke et al.*, 2016] that average values of TEC absolute anomalies were higher before earthquakes than after them. The research [*Ke et al.*, 2016] also showed that negative and positive TEC anomalies during earthquakes with the magnitude of more than 5.0 are not continuous and regular. Moreover, the observed TEC anomalies were proportional to earthquake magnitude and all the anomalies in the epicenters on earthquake days were not significantly higher or lower than on other days [*Ke et al.*, 2016].

Based on TEC data, the authors in [*Budak et al.*, 2024] classified ionospheric disturbances caused by seismic and geomagnetic activities using the k-nearest neighbor algorithm. Earthquakes with the magnitude $M > 5.6$ for the period 1999–2016 were under the consideration. The investigation [*Budak et al.*, 2024] was carried out for two groups. In the first group, events occurred five days before earthquakes were considered and in the second group, events occurred three days before earthquakes were under the study. It was determined [*Budak et al.*, 2024] that 5055 out of 5184 test samples in the first group were classified as true and 129 test samples were false. In the second group 3912 samples were classified as true and 105 as false ones [*Budak et al.*, 2024]. Moreover, the study [*Budak et al.*, 2024] showed that the method accuracy increased in inverse proportion to the distance from the stations to epicenters and in direct proportion to earthquake magnitude.

The paper [*Karatay et al.*, 2025] represents complex spatial-time analysis of ionospheric disturbances associated with seismic activity, applying the algorithm of Differential Rate of TEC (DROT) to GPS data. The research [*Karatay et al.*, 2025] covers ten earthquakes with the magnitudes of 5.6–9.0 and investigates ionosphere variability during pre-seismic, seismic and post-seismic periods as well as during geomagnetically calm and disturbed days. The results [*Karatay et al.*, 2025] showed that ionospheric anomalies are not limited by the earthquake period. Significant anomalies were observed during the seismic events and six days after them [*Karatay et al.*, 2025]. On earthquake days, the DROT values were mainly within the range from 60% to 70% (large-scale disturbances), and on the days, preceding the earthquakes and following them, average-scale disturbances (50%–60%) were observed in the majority of cases [*Karatay et al.*, 2025]. Spatial analysis showed [*Karatay et al.*, 2025] that disturbances are stronger within the radius of 500 km from epicenters and as the distances increase, they become weaker. Thus, the paper [*Karatay et al.*, 2025] confirmed the relation between the processes in the lithosphere, atmosphere and ionosphere and highlighted the impact of seismic processes on the ionosphere.

The hypothesis on the relation between the lithospheric and ionospheric shells was also confirmed by the research [*Tachema*, 2024] in which TEC was analyzed in detail, using the wavelet transform and statistical methods, based on GPS data during a shallow moderate earthquake with the magnitude of 5.1 in Lorca, Spain, on May 11, 2011.

Scientists discuss several physical mechanisms that may cause anomalous changes in the ionosphere before earthquakes [*Hegai et al.*, 2015a]. The paper [*Hegai et al.*, 2023] considers anomalous quasi-static electric field, disturbance of the vertical component of the atmospheric electric field by the Earth surface (E_Z). As illustrated in the paper [*Choudhury et al.*, 2013], the spatial scale of the disturbance area ΔE_Z may reach thousands of kilometers. It has been proved [*Kupovykh*, 1998; *Pestova et al.*, 2014] that this effect is determined by the air surface layer ionization by radon emitted from the Earth crust in the boundary layer. As noted in the paper [*Hegai et al.*, 2023], the scientists [*Kupovykh*, 1998] described two important details concerning the surface layer ionization by radon: 1. at nighttime, due to sudden temperature inversion, a thin layer is formed by the Earth surface where radon concentration is sufficient for negative space charge to form at the height of 0.5–1 m; 2. as the turbulent diffusion or electric field strength grow, the space charge becomes positive. This mechanism explains both positive and negative ionospheric anomalies observed in multiple investigations several days before earthquakes [*Karatay et al.*, 2025; *Ke et al.*, 2016; *Kupovykh*, 1998; *Pulinets and Boyarchuk*, 2004; *Pulinets and Davidenko*, 2018].

Seismogenic electric field, penetrating into the ionosphere is also considered as a mechanism of ionospheric pre-seismic anomaly formation [*Hegai et al.*, 2006, 2015b, 1997; *Kelley et al.*, 2017; *Kuo et al.*, 2011, 2014; *Liu et al.*, 2011; *Pulinets and Boyarchuk*, 2004; *Pulinets et al.*, 2022b]. During different satellite missions [*Chmyrev et al.*, 1997; *Pulinets and Legenka*, 1997; *Zhang et al.*, 2012, 2014], besides electron concentration anomalies, disturbances of electromagnetic field amplitudes were detected in the ionosphere at the altitudes of 500–1000 km before earthquakes. Moreover, electromagnetic disturbances were observed not only in seismically active region, but in conjugated magnetic regions as well [*Chmyrev et al.*, 1997]. The researchers [*Pulinets et al.*, 2002] consider this mechanism as a part of the chain of the seismic-ionospheric relation of the processes initiated by seismogenic electric field on the Earth surface.

It is important to mention the papers [*Pulinets et al.*, 2018a; *Pulinets and Davidenko*, 2018; *Pulinets et al.*, 2015], which describe the model of lithospheric-atmospheric-ionospheric-magnetospheric coupling (LAIC). In the paper [*Pulinets and Davidenko*, 2018], the process of formation of the observed pre-seismic ionospheric anomalies is described in detail and the physical mechanism of generation is suggested. The authors [*Pulinets and Davidenko*, 2018] relate the formation of such anomalies to the behavior of the atmosphere planetary boundary layer during local (night) time. According to the hypothesis [*Pulinets and Davidenko*, 2018], at nighttime, the inverse effect and the low height of the upper boundary of the planetary boundary layer cause accumulation of the radon emitted from the Earth crust in the surface layer. That increases the ionization level and, consequently, increases cluster ion density. This results in the formation of the conditions for strong electric field generation over the region of earthquake preparation [*Pulinets and Davidenko*, 2018]. Moreover, using a series of events with $M \geq 6.0$ in Greece for 2006–2011 and based on the self-similarity property, a method for constructing a pattern (mask) of an ionospheric precursor was proposed in the paper [*Pulinets and Davidenko*, 2018] to automate the procedure of its identification. The method for automated identification of earthquake ionospheric precursor was developed in the research [*Pulinets et al.*, 2021].

A complex approach was used in the paper. It includes both new developments and classical median and statistical methods. The time interval from July 21 to 31, 2025 was considered in detail. During this period, a very strong earthquake with the magnitude $M = 8.8$ (at 23:24:53 UT on July 29, 2025) occurred near the eastern coast of Kamchatka peninsula. Ionospheric critical frequency f_0F_2 data of Paratunka observatory (52.97° N, 158.24° E, Kamchatka peninsula, IKIR FEB RAS) and the data of GPS receivers, included into the regional network of the global navigation satellite system (GNSS) of Kamchatka branch of the Federal Research Center "Geophysical Survey of RAS", were under analysis. In the paper we estimate the values of the absolute vertical total electron content (TEC) taking into account the differential code bias and determine TEC deviations from background level. We also determine and investigate the storminess indexes of vertical variations of the total electron content (WTEC) for the periods of TEC oscillations in the range of 1–10 minutes that corresponds to mid-scale ionospheric disturbances. Detailed analysis was carried out using a new method based on wavelet transform [*Fetisova and Mandrikova*, 2022, 2024; *Mandrikova and Fetisova*, 2020; *Mandrikova et al.*, 2021]. This method applies a generalized multi-component model (GMCM) of ionospheric parameter time variation and computational algorithms built on its basis. GMCM realization makes it possible to detect ionospheric anomalies of different intensity and duration. For the estimates, we applied the introduced measure for anomaly intensity [*Fetisova and Mandrikova*, 2022, 2024; *Mandrikova and Fetisova*, 2020; *Mandrikova et al.*, 2021], characterizing weak, moderate and strong ionospheric disturbances.

Anomalous changes, which characterize intensive oscillation processes in the ionosphere significantly exceeding the background level, were detected in the time series of analyzed ionospheric parameters before and during the considered earthquake on July 29, 2025. Based on the Paratunka observatory data and the data of the GNSS receiver network, a large-scale long (about 2 days) negative anomaly was detected against the background of low geomagnetic activity three days and a half before the earthquake. Investigation results also showed that a large-scale positive anomaly, the intensity of which exceeded the background variations of ionospheric parameters by 3 times and more, was observed during the first day of the aftershock process.

2. Materials and Methods

Method for TEC Determination. A method to determine TEC along the satellite-receiver beam using phase and group measurements at two frequencies is represented in the papers [*Afraimovich and Perevalova*, 2006; *Hofmann-Wellenhof et al.*, 1992]. Based on phase measurements, TEC can be determined at two frequencies [*Hofmann-Wellenhof et al.*, 1992]:

$$I_\phi = \frac{1}{40.308} \frac{f_1^2 f_2^2}{f_1^2 - f_2^2} [(L_1\lambda_1 - L_2\lambda_2) + \text{const} + \sigma L], \quad (1)$$

where $L_1\lambda_1$ and $L_2\lambda_2$ are radio signal phase path increments caused by the phase delay in the ionosphere; $L_1 = \Delta\varphi/2\pi$ and $L_2 = \Delta\varphi/2\pi$ are phase measurements of a GPS receiver, carried out at the frequencies $f_1 = 1575.42$ MHz and $f_2 = 1227.6$ MHz (whole and broken numbers of cycles of ϕ phase), respectively; const is the phase measurement ambiguity; σL is the phase measurement error.

$$I_P = \frac{1}{40.308}\frac{f_1^2 f_2^2}{f_1^2 - f_2^2}[(P_2 - P_1) + \sigma P + \delta P], \tag{2}$$

where P_1, P_2 are group paths for the frequencies f_1 and f_2, respectively, σP is a random error of measurement of distance in code, δP is a systematic error of measurement of distance in code measurements determined mainly by differential code bias $\delta P = c\Delta\tau$, where $\Delta\tau$ is the differential code bias, c is the light velocity.

The Total Electron Content obtained by group measurements is very noisy. This manifests the most significantly at low angles where measurement noise can reach more than 100%. In this case, TEC group measurements are absolute with the accuracy of the error associated with differential code bias. The TEC determination error caused by the differential code bias is determined by the following expression:

$$I_{\text{bias}} = \frac{1}{40.308}\frac{f_1^2 f_2^2}{f_1^2 - f_2^2} c\Delta\tau.$$

To estimate the absolute vertical TEC, we apply TayAbsTEC algorithm [*Yasyukevich et al.*, 2015a,b]. TEC measurement model, used in this algorithm, includes two main components, they are: ionospheric TEC I_{ion} along the satellite-receiver beam and the TEC determined by differential code bias, I_{bias}. Thus, the applied measurement model has the form $I_M = I_{ion} + I_{\text{bias}}$, the parameters of which may be vertical TEC, latitudinal and longitudinal gradients, TEC time derivative:

$$\begin{aligned} I_M = S_i^j\Big\{ & I_{\text{v}}(\varphi_0, l_0, t_0) + G_\varphi \Delta\varphi_j^i + G_{q\varphi}(\Delta\varphi_j^i)^2 \\ & + G_l \Delta l_j^i + G_{ql}(\Delta l_j^i)^2 + G_t \Delta t_j^i + G_{qt}(\Delta t_j^i)^2 \Big\} \\ & + I_{\text{bias}\,j}, \end{aligned} \tag{3}$$

where i is the measurement number, j is the GPS or GLONASS satellite number; I_{v} is the absolute value of vertical TEC; $G_\varphi = \frac{\partial I_{\text{v}}}{\partial \varphi}$, $G_l = \frac{\partial I_{\text{v}}}{\partial l}$, $G_{q\varphi} = \frac{\partial^2 I_{\text{v}}}{\partial \varphi^2}$, $G_{ql} = \frac{\partial^2 I_{\text{v}}}{\partial l^2}$ are linear and quadratic terms of TEC spatial gradients with respect to latitude and longitude; $\Delta\varphi$, Δl are the latitudinal and longitudinal distances between under-ionospheric point and a station; Δt is the time difference between current time t_0 and the midpoint of the interval under analysis; $G_t = \frac{\partial I_{\text{v}}}{\partial t}$, $G_{qt} = \frac{\partial^2 I_{\text{v}}}{\partial t^2}$ are the first and the second time derivatives of TEC.

Model (3) parameters are determined by the least square method. Absolute vertical TEC was calculated with the time interval of 15 minutes.

Data Analysis Methods. To detect TEC anomalous changes in ionospheric parameters, three approaches were used: 1. ionospheric parameter (TEC values and ionosonde data) relative deviations from median values were estimated and ionospheric parameter deviations from background value range were determined on the basis of interquartile range; 2. the algorithm based on the generalized multi-component model of ionospheric parameter time series was applied [*Fetisova and Mandrikova*, 2022, 2024; *Mandrikova and Fetisova*, 2020; *Mandrikova et al.*, 2021]; 3. disturbance index of TEC vertical variations (WTEC) was estimated [*Perevalova et al.*, 2016; *Voeykov et al.*, 2016].

1. Calculation of the deviations of ionospheric parameters from background values was performed using the median method. Median values were estimated over a sliding time window of 27 days (the processing was made “to the past” from the present

moment to eliminate the impact of possible seismic-ionospheric effect). Relative deviations of TEC from background (median) values were determined using the formula:

$$\Delta\text{TEC} = \frac{\text{TEC}_i - \text{TEC}_{\text{med}}}{\text{TEC}_{\text{med}}}, \tag{4}$$

where ΔTEC is the relative deviation of TEC from background values, TEC_i is the current TEC values at time $t = i$; TEC_{med} is the median TEC values. The relative deviation $\Delta f_{\text{o}}F_2$ of the critical frequency from the median values was calculated similarly.

Deviations of ionospheric parameters from the background distribution on the basis of interquartile range were determined from the ratio:

$$Y_{\pm} = \text{X}_{\text{med}}(t_i) \pm 1.5IQR(t_i), \tag{5}$$

where $X_{\text{med}}(t_i)$ are median values of the ionospheric parameter (TEC or $f_{\text{o}}F_2$) calculated in a sliding time window with the duration of 27 days, $IQR(t_i) = Q_3(t_i) - Q_1(t_i)$ is the difference between the upper Q_3 and the lower Q_1 quartiles calculated in the same time window. According to the paper [*Encyclopedia...*, 1982], in case of normal distribution of the values $\Delta X(t_i) = X(t_i) - X_{\text{med}}(t_i)$, the value $1.5IQR(t_i)$ will correspond to about two standard deviations, and the values $X(t_i)$ should vary within the boundaries of the range $Y_{\pm}(t_i)$ with the probability of 95% under the impact of different random factors. Thus, the ionospheric parameter $X(t_i)$ values within the range $Y_{\pm}(t_i)$ may be referred to anomalous values. The hypothesis of normal distribution of the $\Delta X(t_i)$ value was tested using the Jarque-Bera test for a given significance level of $\alpha = 0.05$. The critical value for the Jarque-Bera test at a significance level of $\alpha = 0.05$ is $JB_{crit} = 5.99$. According to the obtained test results, the statistics values JB for the $f_{\text{o}}F_2$ and TEC parameters did not exceed JB_{crit} (in particular, for the critical frequency $f_{\text{o}}F_2$, the statistics value was $JB = 4.45$). According to the test results, the hypothesis of normal distribution of the $\Delta X(t_i)$ value for the $f_{\text{o}}F_2$ and TEC parameters is assumed in this paper with a significance level of $\alpha = 0.05$.

2. The generalized multi-component model (GMCM) of ionospheric parameter time series has the form [*Mandrikova et al.*, 2014]:

$$f(t) = R(t) + A(t) + e(t) = \sum_{\mu} s^{\mu}(t) + \sum_{i} a^{i}(t) + e(t). \tag{6}$$

In model (6), the component $R(t) = \sum_{\mu} s^{\mu}(t)$ describes regular period variations of ionospheric parameters. This component is not used in this research. It is described in detail in the papers [*Mandrikova and Fetisova*, 2020; *Mandrikova et al.*, 2021].

The component $A(t) = \sum_i a^i(t)$ of model (6) describes anomalous changes (increases and decreases) of ionospheric parameters of different intensity, the components $a^i(t) = \sum_{\eta,n} P^i_{\eta,n}(d_{\eta,n})\Psi_{\eta,n}(t)$ are determined through the threshold functions:

$$P^i_{\eta,n}(d_{\eta,n}) = \left[\begin{array}{l} \begin{cases} d^{1+}_{\eta,n}, & \text{if } P^1_{\eta,n} < (d_{\eta,n} - d^{\text{med}}_{\eta,n}) \le P^2_{\eta,n} \\ 0, & \text{if } \left|d_{\eta,n} - d^{\text{med}}_{\eta,n}\right| < P^1_{\eta,n} \text{ or } \left|d_{\eta,n} - d^{\text{med}}_{\eta,n}\right| > P^2_{\eta,n} \\ d^{1-}_{\eta,n}, & \text{if } -P^2_{\eta,n} < (d_{\eta,n} - d^{\text{med}}_{\eta,n}) \le -P^1_{\eta,n} \end{cases} \\ \begin{cases} d^{2+}_{\eta,n}, & \text{if } P^2_{\eta,n} < (d_{\eta,n} - d^{\text{med}}_{\eta,n}) \le P^3_{\eta,n} \\ 0, & \text{if } \left|d_{\eta,n} - d^{\text{med}}_{\eta,n}\right| < P^2_{\eta,n} \text{ or } \left|d_{\eta,n} - d^{\text{med}}_{\eta,n}\right| > P^3_{\eta,n} \\ d^{2-}_{\eta,n}, & \text{if } -P^3_{\eta,n} \le (d_{\eta,n} - d^{\text{med}}_{\eta,n}) < -P^2_{\eta,n} \end{cases} \\ \begin{cases} d^{3+}_{\eta,n}, & \text{if } (d_{\eta,n} - d^{\text{med}}_{\eta,n}) > P^3_{\eta,n} \\ 0, & \text{if } \left|d_{\eta,n} - d^{\text{med}}_{\eta,n}\right| < P^3_{\eta,n} \\ d^{3-}_{\eta,n}, & \text{if } (d_{\eta,n} - d^{\text{med}}_{\eta,n}) < -P^3_{\eta,n} \end{cases} \end{array}\right., \tag{7}$$

where $d_{\eta,n} = \langle f, \Psi_{\eta,n} \rangle$ are the wavelet coefficients, Ψ is the wavelet, η is the scale parameter, n is the time parameter, $\langle \cdot \rangle$ is the scalar product; the thresholds are $P^i_{\eta,n} = V^i \sqrt{\frac{1}{\Phi-1} \sum_{n=1}^{\Phi} (d_{\eta,n} - \overline{d_{\eta,n}})^2}$, where $d^{\text{med}}_{\eta,n}$ and $\overline{d_{\eta,n}}$ are the median and the average value, respectively; the superscript $i = 1\pm; 2\pm; 3\pm$ determines positive and negative anomalies of three classes: class 1 – low intensity; class 2 – moderate intensity; class 3 – high intensity. The thresholds $P^i_{\eta,n}$, determining class anomalies, were estimated by minimizing a posterior risk function [*Levin*, 1989].

Application of operations (7) to the ionospheric critical frequency f_oF_2 data and TEC values, as shown in papers [*Fetisova and Mandrikova*, 2022, 2024; *Mandrikova and Fetisova*, 2020; *Mandrikova et al.*, 2021], makes it possible to detect electron concentration anomalies in the ionosphere (anomalous increases and decreases).

When performing operations (7), Daubechies 3 wavelet was used [*Daubechies*, 1992]. According to the estimates and the criteria in the paper [*Mandrikova and Polozov*, 2012], this wavelet makes it possible to obtain wavelet transform of ionospheric data with the least error.

The model component $e(t)$ describes natural and industrial noises (hardware failures, industrial bursts etc.).

According to the investigation [*Mandrikova et al.*, 2021], in order to estimate the intensity of the anomalies detected in the data on the basis of threshold functions (7), we used the formula:

$$I^i_n = \sum_{\eta=1}^{A} P^i_{\eta,n}(d_{\eta,n}), \tag{8}$$

where A is the largest scale under consideration.

3. Estimation of the storminess indexes of the vertical variations of the total electron content (TEC) was performed according to [*Perevalova et al.*, 2016; *Voeykov et al.*, 2016]. Variation series of inclined TEC $I_i(t)$ along the beams from the GPS receiver to GPS i-th satellite and the series $\Theta_i(t)$ of position angles of the GPS i-th satellite were the initial data for determining the WTEC index. The series of inclined filtered TEC variations of $dI_i(t)$ are transformed into equivalent vertical values $dIv_i(t) = dI_i(t)\sin(\Theta_i(t))$. Then the TEC oscillation intensity $A_i(t)$ is determined for each series $dIv_i(t)$. For this purpose, $dIv_i(t)$ values are taken in absolute values and smoothed by a sliding average with the window lasting for T:

$$A_i(t) = \frac{1}{T} \int_{-T/2}^{T/2} |dIv_i(t+\tau)|\, d\tau.$$

Then for each time moment t, the intensity of TEC variations WTEC(t) is estimated. It is averaged over all the receiver-satellite radio beams for a selected GPS receiver. The procedure of weighted averaging of the series $A_i(t)$ is used in the method:

$$\text{WTEC}(t) = \frac{\sum_{i=1}^{N} A_i(t) S_i(t)}{\sum_{i=1}^{N} S_i(t)}, \tag{9}$$

where N is the satellite number; $A_i(t)$ and $S_i(t)$ are the TEC variation intensity series and weight function for the i-th satellite. The function $S_i(t) = \sin 2(\pi(t - t_{0,i})/\Delta T_i)$ was used as weight function, where ΔT_i is the duration of the corresponding intensity series $A_i(t)$, and $t_{0,i}$ is its beginning.

Data Sources. The study analyzed data from five GPS receivers (KBG, KMSH, KOZS, PAUJ, PETS) included in the regional GNSS receiver network KAMNET of the Kamchatka

Branch of the Federal Research Center "Geophysical Survey of RAS" (https://www.emsd.ru/geodin/regkamnet), as well as data from an ionospheric station "Parus-A" located on the territory of the geophysical observatory of the Institute of Cosmophysical Research and Radio Wave Propagation FEB RAS ($\varphi = 52.97°$ N, $\lambda = 158.24°$ E). Critical frequency f_oF_2 values and trace characteristics on the ionograms, used in this investigation, were obtained during manual processing of the ionograms according to URSI instructions on ionogram interpretation and processing (https://repository.library.noaa.gov/view/noaa/1013). To analyze the geomagnetic activity level, we used the K index obtained at Paratunka geomagnetic observatory ($\varphi = 52.97°$ N, $\lambda = 158.25°$ E) (https://data.www.ikir.ru/webappfiles/gfo_paratunka/pet-kindex.txt), as well as the AE (https://wdc.kugi.kyoto-u.ac.jp/aedir/index.html) and Dst (https://wdc.kugi.kyoto-u.ac.jp/dstdir/index.html) indices published by the World Data Center for Geomagnetism (Kyoto, Japan). Earthquake catalog provided by the United States Geological Survey's (USGS) Earthquake Hazards Program (https://earthquake.usgs.gov/earthquakes/search/) was used in the work. Figure 1 shows the location of the stations whose data were analyzed in the study, and also indicates the epicenter of the earthquake with a magnitude of $M = 8.8$, which occurred on July 29, 2025. For each GPS receiver, slant TEC values with a time step of 30 seconds were determined

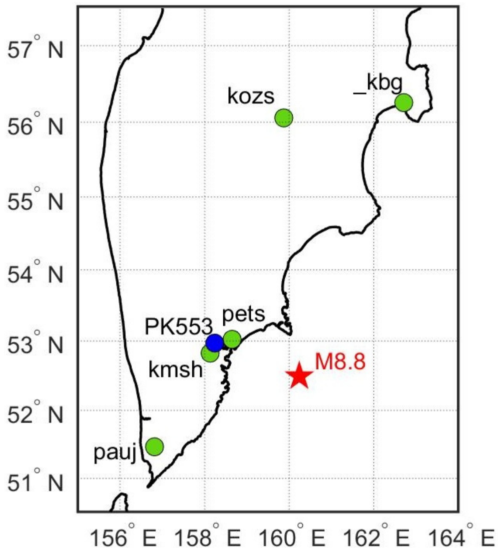

Figure 1. Map showing the locations of GPS receivers (green circles) and an ionospheric station PK553 (blue circle) on the Kamchatka region. The epicenter of the $M = 8.8$ earthquake that occurred on July 29, 2025, is marked with a red star.

from phase and pseudorange measurements using relations (1) and (2). Using model (3), absolute vertical TEC values I_v were calculated from slant TEC values with a time step of 15 minutes. The obtained I_v values were then analyzed using the methods presented in relations (4)–(8). Using the same relations, 15-minute values of the critical frequency f_oF_2 were analyzed in this study. Using the slant TEC values, the WTEC index was calculated using (9) to estimate the intensity of TEC oscillations in the 1–10 minute period range, which correspond to mid-scale ionospheric disturbances.

3. Results and Discussion

The results of ionospheric parameter time series processing for the period July 21–31, 2025 are illustrated in Figure 2–4. According to FSBI "IAG" data (http://ipg.geospace.ru/space-weather-review/), the integral solar activity over the analyzed period was assessed as moderate. Solar flare activity was assessed as low. The number of sun spots SN changed from 106 to 191, the radio radiation flux at the wavelength of $\lambda = 10.7$ cm was from 139 to 156 pfu ($10^{-22} \cdot W \cdot m^{-2} \cdot Hz^{-1}$). Figure 2 shows the results of ionospheric data processing based on ratios (4), (5). As it was described above, classical median method was applied. The results of the processing of the ionosonde data from Paratunka observatory (Kamchatskiy kray, ionospheric critical frequency f_0F_2 data were processed) are illustrated in Figure 2a,b. The results of data processing from the GPS receivers of the regional GNSS network are presented in Figure 2c–l (data from KBG, KMSH, KOZS, PAUJ, PETS receivers were processed). To analyze geomagnetic activity, Figure 2m–o shows K index values (Paratunka observatory data, measurements are made by IKIR FEB RAS) and Dst and AE indices values (WDC for Geomagnetism (Kyoto, Japan)). Analysis of the results in Figure 2 shows that during the insignificant increase of geomagnetic activity on July 22–24, 2025 (on July 22, 2025 the daily total K index value is $\sum K = 22$; on July 23 and 24, 2025, the day total K index value is $\sum K = 24$, AE index on these days exceeded 600 nT), positive anomalous deviations (marked with red on all graphs) are observed in ionospheric parameters according to ionosonde data and the data of all the GPS receivers under analysis.

The highest amplitude deviations of ionospheric parameters from median values (green graphs in Figure 2) are observed in f_0F_2 data and in TEC data when the Dst index reached its minimum values (Figure 2n), that is the end of the day on July 23 and the first half of the day on July 24. Insignificant short-time positive anomalous deviations are also observed on July 25 and 26, 2025 during weak increase of AE index (AE index maximum was 400 nT on July 25 and 500 nT on July 26). The observed dynamics of the ionospheric parameters during the geomagnetic activity increase is standard according to our earlier investigations [*Fetisova and Mandrikova*, 2022, 2024; *Mandrikova and Fetisova*, 2020; *Mandrikova et al.*, 2021] and the investigations of other researchers [*Danilov and Konstantinova*, 2023; *Tsagouri*, 2022]. We should also note that significant deviation of ΔTEC in the analyzed data is observed at the end of the day on July 22 before geomagnetic activity increase. Anomalous increases in the ionospheric parameters preceding the periods of increased geomagnetic activity were mentioned in a number of papers [*Danilov and Konstantinova*, 2023; *Fetisova and Mandrikova*, 2024; *Mandrikova et al.*, 2021; *Tsagouri*, 2022]. They are of interest and are actively investigated in the field of space weather tasks.

Analysis of the results in Figure 2 shows that positive anomalous changes are observed in ionospheric parameters at the earthquake moment on July 29–31 (according to the data of KBG, PAUJ and PETS receivers) and during a long period of the aftershock process on July 30 and 31. The deviations are observed at local time moments in all the analyzed data. We should note that during that period the geomagnetic field was calm (Figure 2m), three-hour K index values at Paratunka observatory did not exceed $K = 2$. Geomagnetic activity of the auroral zone at the time of the earthquake was also weak (AE index did not exceed 200 nT). During the aftershock process, the AE index had the values of 300–400 nT at some intervals of time. The result shows the relation of the detected anomalous changes with seismic process.

Figure 3 shows the results of ionospheric parameter processing. They were performed on the basis of a new method for data analysis using a generalized multi-component model (GMCM) [*Mandrikova and Fetisova*, 2026; *Mandrikova et al.*, 2014] (ratios (6)–(8)). GMCM application made it possible to investigate the ionospheric parameter dynamics in detail, detect anomalous changes and estimate their intensity. Development of the GMCM and estimation of its parameters were carried out according to the data of the vertical radio sounding of the ionosphere obtained at Paratunka observatory (Kamchatskiy kray, IKIR FEB RAS). The threshold function parameters of the GMCM (ratio 7) were determined by minimizing a posterior risk [*Levin*, 1989], which was estimated by using the data of three classes: class 1 – ionospheric parameter variations during geomagnetically calm conditions; class 2 – ionospheric parameter variations during increased geomagnetic activity and magnetic storms; class 3 – ionospheric parameter variations during periods of strong geomagnetic activity and geomagnetic storms. According to the considered classes, when estimating the GMCM parameters, we minimized the risk for the problem of detection of ionospheric anomalies occurring during increased geomagnetic activity and geomagnetic storms. Analysis of the GMCM results during increased seismic activity in

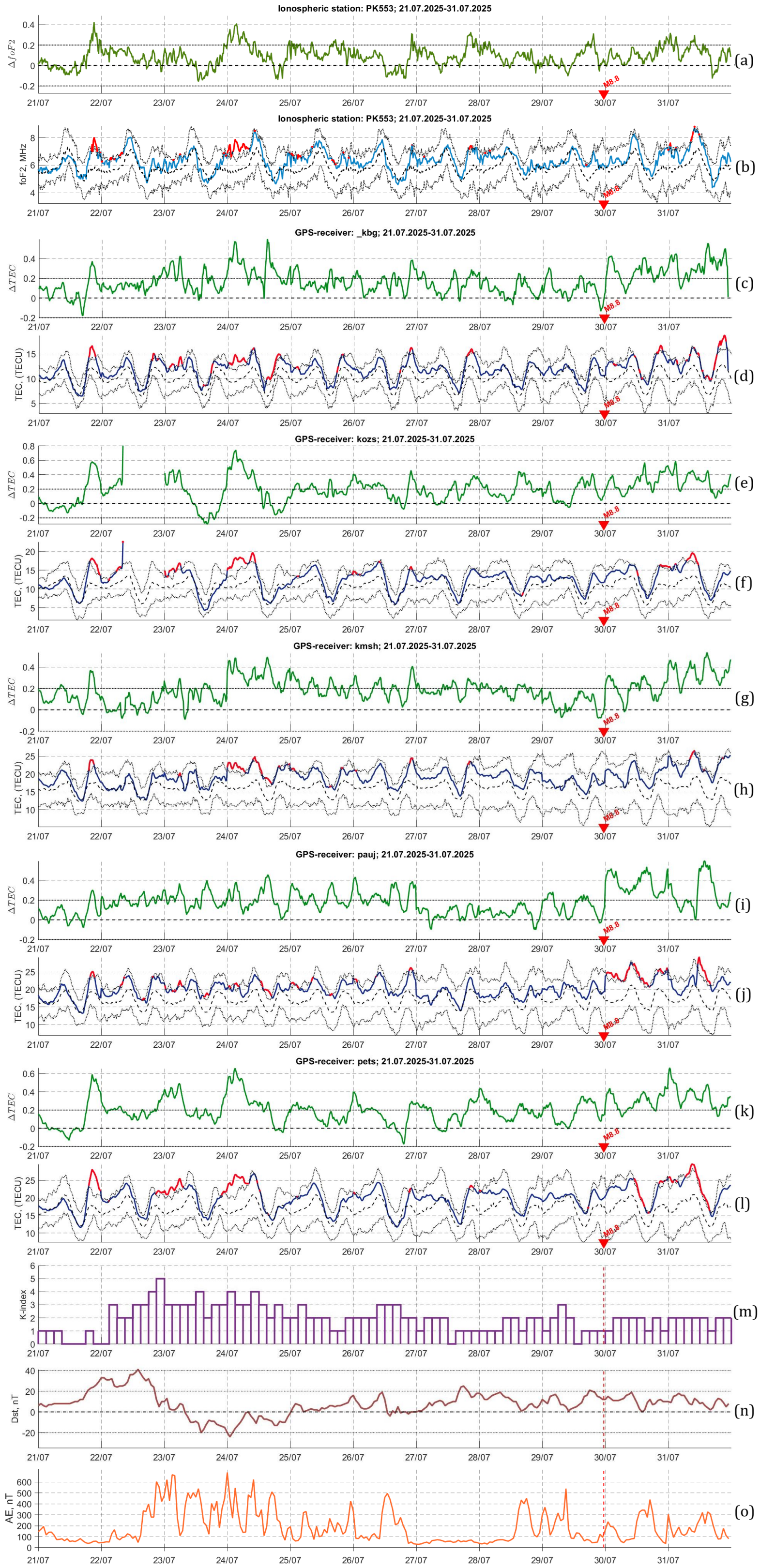

Figure 2. Values of Δf_oF_2 and ΔTEC (green lines), f_oF_2 and TEC values (blue lines), median values (dashed lines), the lower and upper boundaries of the background range (dashed lines); f_oF_2 and values outside the background range boundaries, determined at the confidence probability of 95% are shown in red.

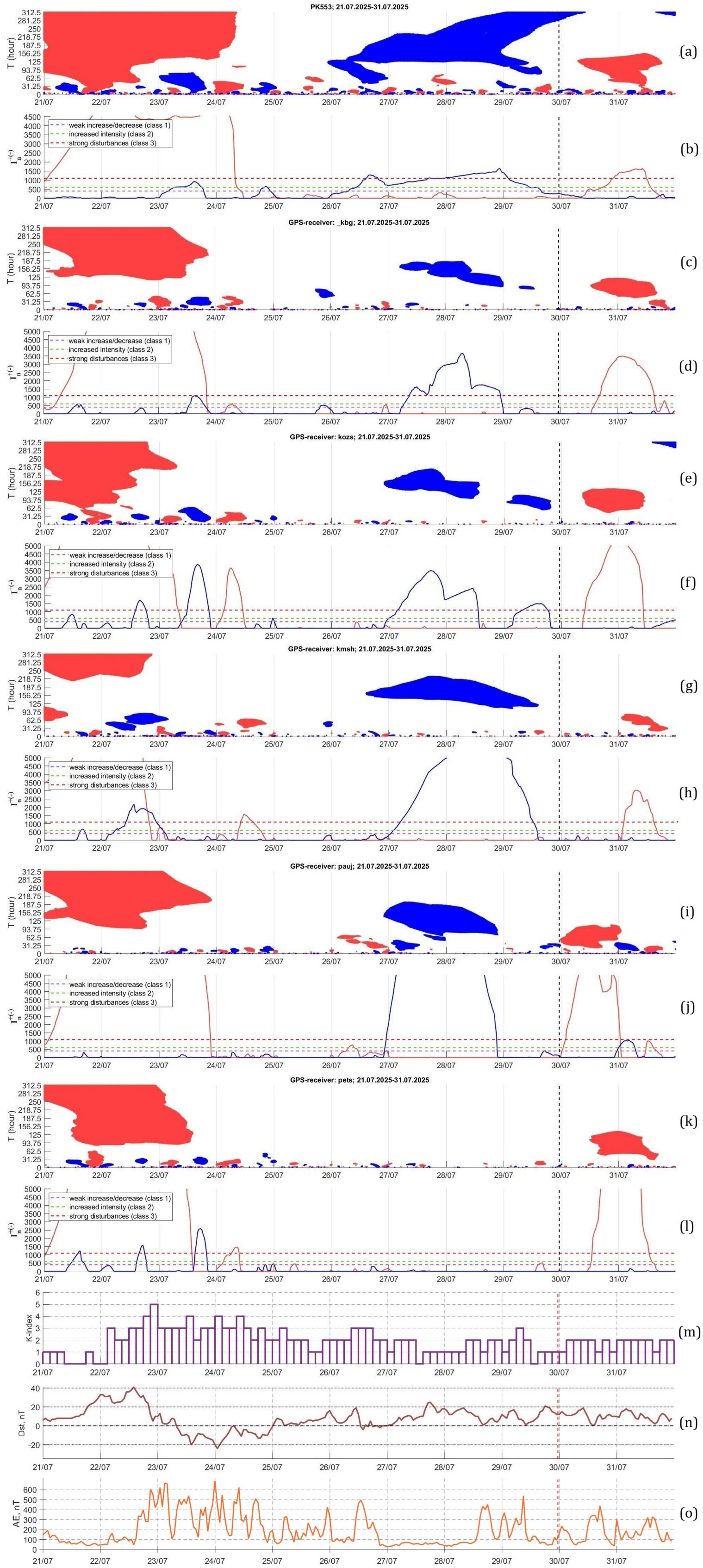

Figure 3. Results of anomaly detection in ionospheric data based on GMCM method. The black and red vertical dashed lines indicate the time of earthquake occurrence with the magnitude of $M = 8.8$.

Kamchatka [*Mandrikova and Fetisova*, 2026] using the data over a long time interval (data for 2000–2023 were under analysis) showed that oscillation processes of low intensity can be observed in f_oF_2 data before earthquakes with the magnitude $M = 5$ in Kamchatka. These oscillation processes can be positive or negative anomalous changes significantly exceeding the background level according to GMCM parameters. During earthquakes and just after them, more intensive and long anomalous changes in ionospheric parameters can be observed. In the majority of cases, they characterize anomalous increases of ionospheric electron concentrations. These anomalies can be accompanied by significant changes in f_oF_2 data time variation. According to these results, f_oF_2 during the period under analysis was processed using lower thresholds (Figure 3a,b, positive anomalies are red, negative are blue).

Analysis of f_oF_2 processing results shows that oscillation processes occurred in the ionosphere on July 22–24 at the background of insignificant increase of geomagnetic activity. General background of f_oF_2 was significantly increased, long positive anomaly (class 3 for GMCM with lower thresholds) was observed. Oscillation processes in the ionosphere on July 22–24 are also confirmed by the results obtained from TEC data (Figure 3). Comparison of the results (colored graphs in Figure 3) shows a general character of the ionospheric process during that period and indicates their validity. We should note that positive anomaly in TEC is clearly visible in the data from all GPS receivers. We should also note that the GMCM results agree well with the results of the median method. However, they make it possible to investigate the frequency-time structure of ionospheric data more in detail.

Results in Figure 3 show that long negative anomaly (marked with blue) was formed in the ionosphere before the earthquake. According to f_oF_2 data, the anomaly occurred three days and a half before the earthquake and had low intensity (class 1 according to GMCM parameters). This anomaly is also observed in the data of KBG, KOZS, KMSH and PAUJ receivers (Figure 3c-j), but it is the most clearly observed in PAUJ data (Figure 3i,j). Exceedence of thresholds, according to PAUJ data, corresponds to the very intensive negative ionospheric disturbances (exceeds class 3) on July 27 and 28. According to the data from the KBG and KOZS receivers, it is clear that the greatest intensity of the anomaly is achieved at night local time. Note that during the negative anomaly formation and the highest values of its intensity, the geomagnetic field was calm (three-hour values of K-index at Paratunka observatory did not exceed $K = 2$, AE index was less than 100 nT). The general character of the ionospheric process during the pre-seismic period, observed according to the data of different measurements, indicates the validity of these results.

The observed anomalous dynamics in ionospheric parameters completely agrees with lithospheric-atmospheric-ionospheric-magnetospheric coupling (LAIC) model, described in the papers [*Pulinets and Davidenko*, 2018; *Pulinets et al.*, 2015]. According to this model, formation of such anomalies is associated with the behavior of the atmospheric planetary boundary layer at local (night) time [*Pulinets and Davidenko*, 2018]. As it was mentioned in the introduction, based on the results of the paper [*Pulinets and Davidenko*, 2018], radon emitted from the Earth crust in the area of earthquake preparation may be accumulated in the boundary layer during nighttime. As the result, ionization level increases and, consequently, cluster ion density grows, electric properties of the Global electric circuit also change that may further cause formation of large-scale positive and negative anomalies in the ionosphere. Moreover, the obtained results are consistent with the investigation [*Liperovskaya et al.*, 2006; *Romanovskaya and Namgaladze*, 2014]. In the study [*Romanovskaya and Namgaladze*, 2014] the periods of strong earthquakes in 2005 were analyzed using regional maps of relative disturbances of the ionospheric TEC. Negative anomalies in the TEC before the seismic events in Iran on February 22, 2005 and in Indonesia on February 26, 2005 had a similar character. Researchers [*Romanovskaya and Namgaladze*, 2014] suggested that the most probable physical mechanism for the formation of such anomalies is the vertical electromagnetic $E \times B$ drift of the F_2-region plasma, caused by an electric field of seismic origin, which changes the concentration of electrons above the epicentral region and in the magnetically conjugate zone [*Namgaladze et al.*, 2009]. We should note that application of the median method (Figure 2) did not allow us to detect this anomaly in ionospheric parameters. This indicates higher sensitivity of the GMCM method. GMCM method sensitivity is explained by high detecting capability of wavelets providing the amplitude increase by 1.5–1.8 times (depending on the applied wavelet function) in the vicinity of the peculiarities (anomalies) in the data. It should also be noted that the negative anomaly is not highlighted in the PETS receiver data, which indicates the need for development of the GNSS network.

At the moment of earthquake occurrence and during the aftershock process development, long positive anomaly was formed in the ionosphere according to the results of f_oF_2 and TEC. In the data of different GPS receivers, the periods of anomalous threshold exceedance have some time shifts, however the process dynamics is common. The result agrees with the median method (Figure 2).

To investigate the ionosphere state during the preparation and occurrences of strong earthquakes with $M = 8.8$, we analyzed vertical sounding ionograms from Paratunka observatory. This analysis showed the presence of a series of ionospheric anomalies, some of which were observed at the background of geomagnetically calm conditions ($K \leq 2$–3). This allows us to consider these anomalies in the ionosphere as possible manifestations of lithospheric-ionospheric coupling.

Before the earthquake, during the fore-shock activation beginning on July 21, 2025, when the geomagnetic activity was low (summary diurnal K index was $\sum K = 4$, the average diurnal $AE = 86$ nT, $AE_{\max} = 193$ nT, $Dst_{\min} = 6$ nT), a sporadic layer E_s of type r was recorded on the ionograms in E region during the time interval 11:30–11:45, as well as the E_s-spread was observed during the periods 01:00–02:00 and 07:15–07:45. In F region, the F-spread was recorded during the period 13:00–16:00, frequency and virtual height (type H) stratification of the trace in F_2 was observed at 00:45, 01:15, 01:45, 02:30, 03:00, 03:45, 04:45, 05:00, 21:30, 22:30 and 22:45. Based on the USGS catalog data, eight seismic events with the magnitude $5.0 \geq M < 5.5$ were recorded during the day on July 21, 2025 near the eastern coast of the Kamchatka. Ionograms with marked features of the trace of reflections of an ordinary wave recorded at 11:30 UT and 15:45 UT are shown in Figure 4. From July

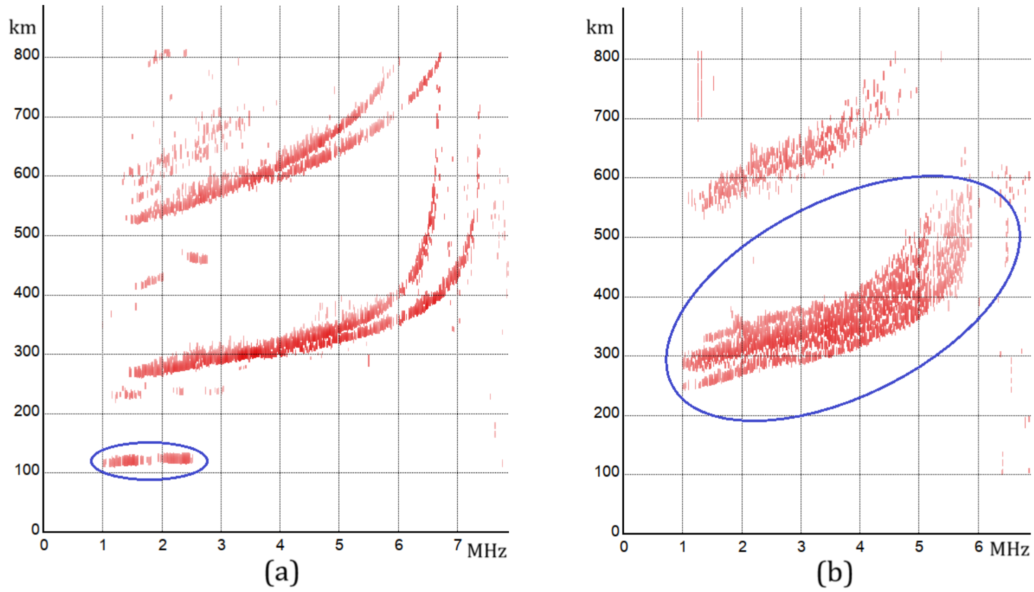

Figure 4. Ionograms of the ionospheric station of the Paratunka observatory, obtained on July 21, 2025, with the noted features of the trace of ordinary wave reflections: (a) sporadic layer E_s of type r at 11:30 UT (23:30 LT); (b) F-spread at 15:45 UT (July 22, 2025 at 03:45 LT).

22 to 26, 2025 increased geomagnetic activity was observed. In particular on July 22, 23, 24 and 26, 2025, the summary diurnal K-index had the values $\sum K = 22$, $\sum K = 24$, $\sum K = 24$ and $\sum K = 19$, respectively. Screening of F region, E_s-spread, sporadic layer E_s of type r, trace stratification and branching in F_2 region were recorded on the ionograms during that period. The detected anomalies were probably the responses on geomagnetic disturbances and cannot be directly interpreted as manifestations of seismic activity. According to the USGS catalog data, sixteen seismic events with the magnitude $5.0 \geq M < 6.0$ were recorded from July 22 to 26, 2025 near the eastern coast of Kamchatka.

During the day on July 27, 2025, when the geomagnetic activity was low (the summary diurnal K index was $\sum K = 10$, average diurnal $AE = 54$ nT, $AE_{\max} = 72$ nT, $Dst_{\min} = 0$ nT), we recorded E_s-spread at 15:30–16:00, frequency and virtual height (type H) stratification of the trace in the layer F_2 at 01:30, trace branching near the critical frequency (type V) at 00:45, 01:15, 17:15, 19:00, 21:00, abnormal variation of the trace near the critical frequency (type Y) at 22:30, F-spread at 17:00, Z-component at 17:15 and 19:00. Ionograms with marked features of the trace of reflections of an ordinary wave recorded at 15:45 UT and 19:00 UT are shown in Figure 5. We should note that the intensity of the negative ionospheric anomaly considered above during that period reached the highest values according to the results of TEC and f_oF_2 (Figure 3a–i). Based on the USGS catalog data, during the day on July 27, 2025, no seismic events with the magnitude $M \geq 5$ were recorded near the eastern coast of Kamchatka. Low geomagnetic activity also remained during

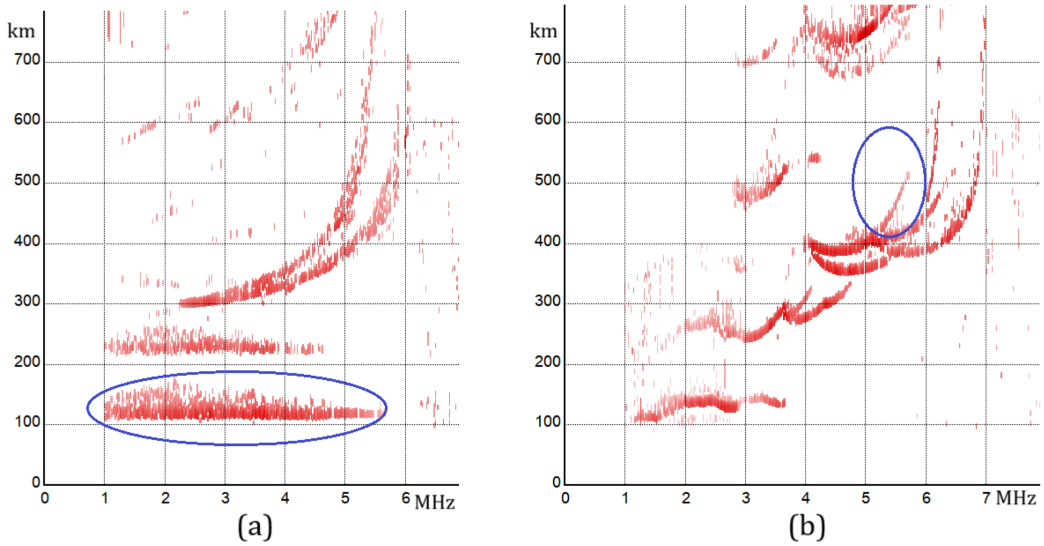

Figure 5. Ionograms of the ionospheric station of the Paratunka observatory, obtained on July 27, 2025, with the noted features of the trace of ordinary wave reflections: (a) E_s-spread at 15:45 UT (July 28, 2025 at 03:45 LT); (b) Z-component at 19:00 UT (July 28, 2025 at 07:00 LT).

the day on July 28, 2025 ($\sum K = 12$, the average diurnal $AE = 145$ nT, $AE_{\max} = 451$ nT, $Dst_{\min} = 1$ nT). On the ionograms on July 28, 2025, we recorded the sporadic layer Es of type r at 12:45–13:00, E_s-spread during the time intervals 08:30, 10:00–11:00, 16:00–16:15, 17:45–18:30, screening of F region (type A) at 00:15, frequency and virtual height (type H) stratification of the trace in F_2 layer at 00:30, 01:30, 02:15, 03:15, 21:45 and 22:30, trace branching near the critical frequency (type V) at 03:30, 18:15, 18:30, 20:00, 20:30, abnormal variation of the trace near the critical frequency (type Y) at 04:15, 19:00, 19:15, 19:30, Z-component at 21:00. As it follows from the results presented above (Figure 3), the intensity of the negative ionospheric anomaly during these days was also very high (significantly exceeded the threshold of class 3). According to the USGS catalog data, one seismic event with the magnitude $M = 5.1$ was recorded at 11:45 UT near the eastern coast of Kamchatka.

Thus, during the precursor period, which began on July 20, 2025 (9 days before the main event), ionospheric disturbances reached their maximum on July 27–28, 2025. Under the conditions of absence of any seismic events with $M \geq 5.0$ and low geomagnetic activity on July 27, 2025, we recorded sporadic layer E_s of type r and trace diffusivity in E region, long diffusivity of the trace in F region, large number of rare forms of traces (V, Y, Z), indicating the presence of steep horizontal gradients of electron concentration. On the following day, July 28, 2025, the general geomagnetic state was calm in spite of the small increase in sub-storm activity during the second half of the day. A dense layer of electron concentration (screening layer E_s) was recorded in E region at midday LT and a diffusive sporadic layer (E_s-spread) and of type r were recorded during evening and night hours LT. In F region, stratification (type H) and traces of types V and Y were multiply recorded indicating the presence of strong inclinations of ionospheric layers. The Z-component recorded during morning hours LT emphasizes the presence of steep gradients of electron density.

Analysis of the ionograms for July 29, 2025 allowed us to divide the anomalies into two types: pre-seismic Z-component (15:45 LT) and E_s-spread (02:15 and 02:30 LT), and the post-seismic anomaly in the form of the trace of type Y recorded 21 minutes after the main shock which is possibly caused by the AGW arrival from the earthquake epicenter. The aftershock period (July 30–31, 2025) was accompanied by intensive post-seismic anomalies. In the E region, a diffusive sporadic layer E_s and E_s of type r were recorded at nighttime LT and a screening layer E_s was recorded during daytime. In the F region, long diffusivity of the layer (F-spread) was observed during evening and night hours indicating the presence of large-scale wave disturbances. During morning hours LT, stratification (type H) and branching (type V) of traces were multiply observed that indicates vertical wave motions and steep horizontal gradients caused by seismogenic inner gravitational waves. The analysis results for the ionograms agree with the results of processing of f_oF_2 data and TEC data presented above.

Figure 6 shows the results of estimation of storminess indexes for vertical variations of the total electron content (WTEC) according to the data of KBG, KMSH, KOZS, PAUJ, PETS receivers. WTEC index is the averaged value of TEC variation intensity, filtered in a selected period range. WTEC change limits are determined by the limits of TEC oscillation amplitude change, which significantly depend on ionospheric inhomogeneity scales. In the present paper, we considered TEC oscillations, corresponding to mid-scale ionospheric disturbances, in the period range of 1–10 minutes. The earthquake occurrence time is marked in Figure 6 by a red triangle. Analysis of the results in Figure 6 shows that during insignificant increase of geomagnetic activity on July 23–26, local increases of WTEC index (up to the values WTEC $\cong 0.1$) are observed in the frequency range under analysis.

At the moment of earthquake occurrence, a short-term increase of WTEC (up to WTEC 0.1 and more) occurred based on the data from KMSH, PAUJ, PETS receivers (Figure 6c,d,e). We should note that the highest increase of WTEC index is observed according to the PAUJ receiver data, WTEC at the earthquake moment exceeds the value of 0.2. Significant increase of WTEC index is also observed after the earthquake during the second half of the day on July 31. The results agree with the results illustrated in Figure 3 and ionograms data from Paratunka observatory. The results are also consistent with the work [*Astafyeva and Afraimovich*, 2006], in which GPS data were used to identify very intense quasi-periodic disturbances in the total electron content (oscillation period of about 15 minutes) caused by a strong earthquake in Sumatra and the Andaman Islands on December 26, 2004. The researchers [*Astafyeva and Afraimovich*, 2006] suggested that the most likely source of the identified oscillations was a seismic airwave that arose as a result of a sudden vertical displacement of the earth's surface near the epicenter.

Figure 6. Indexes for vertical variations of the total electron content (WTEC) according to the data of KBG, KMSH, KOZS, PAUJ, PETS receivers.

4. Conclusion

Analysis of ionospheric data of Paratunka observatory (52.97° N, 158.24° E, Kamchatka peninsula, IKIR FEB RAS) and the data of the regional GNSS receiver network, performed by different methods, allowed us to detect anomalous changes in ionospheric parameters and to estimate their intensity during a very strong earthquake on Kamchatka peninsula on July 29, 2025. The detected anomalous changes characterize moderate and intensive oscillation processes in the ionosphere exceeding the background level.

Before the earthquake, against the background of calm geomagnetic conditions, a large-scale negative anomaly, occurred three days and a half before the earthquake and, characterizing moderate disturbances, was detected in ionospheric parameter time series. The anomaly occurrence was observed according to the data of different measurements and had a common character that indicates the validity of these results. The pre-seismic anomaly was the most clearly observed in the data of the PAUJ receiver, which is located near the earthquake source with a small shift in the south-western direction. Based on PAUJ data, the exceedance of thresholds corresponded to intensive negative ionospheric disturbances. A new method for ionospheric parameter analysis, based on the application of the GMCM using wavelet decompositions, made it possible to detect the pre-seismic anomaly. Application of the median method did not allow us to detect this anomaly. The result indicates the necessity to develop the methods for data analysis and to extend the tools for ionospheric parameters recording.

Investigation of the ionograms of vertical radio sounding (Paratunka observatory data) showed that during the period of formation and development of the large-scale negative ionospheric anomaly on July 27–28, 2025, ionospheric disturbances reach their maximum. Under the conditions of absence of seismic events with $M \geq 5.0$ and low geomagnetic activity on July 27, 2025 during evening and night hours, we recorded E_s of type r and diffusivity of the trace in E region, long diffusivity of the trace in F region, large number of rare forms of traces (V, Y, Z), indicating the presence of significant horizontal gradients of electron concentration. On the following day on July 28, 2025, a dense layer of electron concentration (screening layer E_s) was recorded in E region at midday and a diffusive sporadic layer (E_s-spread) and E_s of type r were observed during evening and night hours. Stratification (type H) and traces of types V and Y were multiply recorded in F region indicating the presence of strong inclination of ionospheric layers. The Z-component recorded during morning hours LT confirmed the presence of steep gradients of electron density.

At the moment of earthquake occurrence, application of different methods showed formation of the intensive positive anomaly in the ionosphere. Based on the data of KMSH, PAUJ, PETS receivers, short-term increase of WTEC index up to the value WTEC 0.1 and more occurred. The highest increase of the WTEC index was observed in the data of the PAUJ receiver, WTEC at the earthquake moment exceeded the value of 0.2.

According to the data of Paratunka observatory and the data of all the analyzed GNSS receivers, a large-scale positive anomaly, exceeding the background variations in the intensity by three times and more, was formed in the ionosphere against the background of calm geomagnetic field during the aftershock process development. The positive anomaly lasted for about two days.

The results obtained in the paper agree with our earlier investigations [*Fetisova and Mandrikova*, 2024; *Mandrikova and Fetisova*, 2026; *Mandrikova et al.*, 2014] and the results of other researchers and research groups [*Astafyeva and Afraimovich*, 2006; *Budak et al.*, 2024; *Karatay et al.*, 2025; *Ke et al.*, 2016; *Liperovskaya et al.*, 2006; *Liu and Xu*, 2016; *Romanovskaya and Namgaladze*, 2014; *Tachema*, 2024]. Moreover, the investigation results confirmed the validity of the lithospheric-atmospheric-ionospheric-magnetospheric coupling model described in the papers [*Pulinets and Davidenko*, 2018; *Pulinets et al.*, 2015]. According to the studies [*Astafyeva and Afraimovich*, 2006; *Bogdanov and Pavlov*, 2023; *Budak et al.*, 2024; *Fetisova and Mandrikova*, 2024; *Karatay et al.*, 2025; *Ke et al.*, 2016; *Liperovskaya et al.*, 2006; *Liu and Xu*, 2016; *Mandrikova and Fetisova*, 2026; *Mandrikova et al.*, 2014; *Romanovskaya and Namgaladze*, 2014; *Tachema*, 2024], ionospheric disturbance intensity during strong earthquakes may exceed the background level. On the example of the event on July 29, 2025, this investigation showed that ionosphere reaction on seismic processes may have pronounced character and be accompanied by variability of ionospheric parameters exceeding the background values.

Acknowledgments. The paper was supported by the State Task of IKIR FEB RAS (Subject Registration No. 124012300245-2). The authors thank the Kamchatka Branch of the Federal Research Center "Geophysical Survey of RAS" (Petropavlovsk-Kamchatskiy, Russia) for providing data from the regional GPS receiver network KAMNET. The authors thank the Institute of Cosmophysical Research and Radio Wave Propagation FEB RAS (Paratunka, Russia) and the World Data Center for Geomagnetism (Kyoto, Japan) for providing geomagnetic data. The authors also thank the United States Geological Survey's (USGS) Earthquake Hazards Program for providing access to earthquake data.

References

Afraimovich E. L., Astafieva E. I., Gokhberg M. B., et al. Variations of the total electron content in the ionosphere from GPS data recorded during the Hector Mine earthquake of October 16, 1999, California // Russian Journal of Earth Sciences. — 2004. — Vol. 6, no. 5. — P. 339–354. — https://doi.org/10.2205/2004es000155

Afraimovich E. L. and Perevalova N. P. GPS monitoring of the Earth's Upper Atmosphere. — Irkutsk : SC RRS SB RAMS, 2006. — 480 p. — (In Russian).

Astafyeva E. I. and Afraimovich E. L. Long-distance traveling ionospheric disturbances caused by the great Sumatra-Andaman earthquake on 26 December 2004 // Earth, Planets and Space. — 2006. — Vol. 58, no. 8. — P. 1025–1031. — https://doi.org/10.1186/bf03352607

Bilitza D., Pezzopane M., Truhlik V., et al. The International Reference Ionosphere Model: A Review and Description of an Ionospheric Benchmark // Reviews of Geophysics. — 2022. — Vol. 60, no. 4. — https://doi.org/10.1029/2022rg000792

Bogdanov V. and Pavlov A. Disturbances in E and F Layers of the Ionosphere Preceding Earthquakes in the Kamchatka Region // Solar-Terrestrial Relations and Physics of Earthquake Precursors. — Cham : Springer Nature Switzerland, 2023. — P. 245–254. — https://doi.org/10.1007/978-3-031-50248-4_25

Bolsunovskii M. A., Shestakov N. V., Dolgikh G. I., et al. Ionospheric disturbances over Primorsky Krai caused by the eruption of the Hunga Tonga-Hunga Ha'apai volcano on January 15, 2022 // Geodynamics & Tectonophysics. — 2024. — Vol. 15, no. 1. — P. 0738. — https://doi.org/10.5800/gt-2024-15-1-0738 — (In Russian).

Bošková J., Šmilauer J., Třiska P., et al. Anomalous behaviour of plasma parameters as observed by the intercosmos 24 satellite prior to the iranian earthquake of 20 June 1990 // Studia Geophysica et Geodaetica. — 1994. — Vol. 38, no. 2. — P. 213–220. — https://doi.org/10.1007/bf02295915

Budak C., Karatay S., Erken F., et al. Classification of the Ionospheric Disturbances Caused by Geomagnetic and Seismic Activity with K-Nearest Neighbors Algorithm // Wireless Personal Communications. — 2024. — Vol. 134, no. 3. — P. 1551–1569. — https://doi.org/10.1007/s11277-024-10965-z

Chmyrev V. M., Isaev N. V., Serebryakova O. N., et al. Small-scale plasma inhomogeneities and correlated ELF emissions in the ionosphere over an earthquake region // Journal of Atmospheric and Solar-Terrestrial Physics. — 1997. — Vol. 59, no. 9. — P. 967–974. — https://doi.org/10.1016/s1364-6826(96)00110-1

Choudhury A., Guha A., De B. K., et al. A statistical study on precursory effects of earthquakes observed through the atmospheric vertical electric field in northeast India // Annals of Geophysics. — 2013. — Vol. 56, no. 3. — R0331. — https://doi.org/10.4401/ag-6235

Danilov A. D. and Konstantinova A. V. F-Region Variations Prior to Magnetic Storms (a Review) // Geomagnetism and Aeronomy. — 2023. — Vol. 63, no. 6. — P. 671–685. — https://doi.org/10.1134/s0016793223600649

Daubechies I. Ten Lectures on Wavelets. — Philadelphia : Society for Industrial, Applied Mathematics, 1992. — 357 p. — https://doi.org/10.1137/1.9781611970104

Depueva A. Kh., Mikhailov A. V., Devi M., et al. Spatial and time variations in critical frequencies of the ionospheric F region above the zone of equatorial earthquake preparation // Geomagnetism and Aeronomy. — 2007. — Vol. 47, no. 1. — P. 129–133. — https://doi.org/10.1134/s0016793207010197

Encyclopedia of statistical sciences. Volume 3 / ed. by S. Klotz and N. L. Johnson. — Hoboken : John Wiley & Sons, 1982. — 736 p.

Fetisova N. V. and Mandrikova O. V. Modeling and analysis of ionospheric parameters based on generalized multi-component model // Vestnik KRAUNC. Fiziko-matematičeskie nauki. — 2022. — Vol. 41, no. 4. — P. 89–106. — https://doi.org/10.26117/2079-6641-2022-41-4-89-106 — (In Russian).

Fetisova N. V. and Mandrikova O. V. Analysis of the Ionospheric Parameter Dynamics During Disturbed Periods Based on Aurora System Results // Vestnik KRAUNC. Fiziko-matematičeskie nauki. — 2024. — Vol. 49, no. 4. — P. 157–170. — https://doi.org/10.26117/2079-6641-2024-49-4-157-170 — (In Russian).

Goncharenko L. P., Tamburri C. A., Tobiska W. K., et al. A New Model for Ionospheric Total Electron Content: The Impact of Solar Flux Proxies and Indices // Journal of Geophysical Research: Space Physics. — 2021. — Vol. 126, no. 2. — https://doi.org/10.1029/2020ja028466

Hegai V., Zeren Z. and Pulinets S. Seismogenic Field in the Ionosphere before Two Powerful Earthquakes: Possible Magnitude and Observed Ionospheric Effects (Case Study) // Atmosphere. — 2023. — Vol. 14, no. 5. — P. 819. — https://doi.org/10.3390/atmos14050819

Hegai V. V., Kim V. P. and Liu J. Y. The ionospheric effect of atmospheric gravity waves excited prior to strong earthquake // Advances in Space Research. — 2006. — Vol. 37, no. 4. — P. 653–659. — https://doi.org/10.1016/j.asr.2004.12.049

Hegai V. V., Kim V. P. and Liu J. Y. On a possible seismomagnetic effect in the topside ionosphere // Advances in Space Research. — 2015a. — Vol. 56, no. 8. — P. 1707–1713. — https://doi.org/10.1016/j.asr.2015.07.034

Hegai V. V., Kim V. P. and Liu J. Y. On a possible seismomagnetic effect in the topside ionosphere // Advances in Space Research. — 2015b. — Vol. 56, no. 8. — P. 1707–1713. — https://doi.org/10.1016/j.asr.2015.07.034

Hegai V. V., Kim V. P. and Nikiforova L. I. A possible generation mechanism of acoustic-gravity waves in the ionosphere before strong earthquakes // Journal of Earthquake Prediction Research. — 1997. — Vol. 6. — P. 584–589.

Hegai V. V., Legen'ka A. D., Kim V. P., et al. Wave-like perturbations in the ionospheric F2-layer observed after the Ms8.1 Samoa earthquake of September 29, 2009 // Advances in Space Research. — 2011. — Vol. 47, no. 11. — P. 1979–1982. — https://doi.org/10.1016/j.asr.2011.01.011

Hofmann-Wellenhof B., Lichtenegger H. and Collins J. Global Positioning System. — New York : Springer Vienna, 1992. — 326 p. — https://doi.org/10.1007/978-3-7091-5126-6

Ivanov V. A., Zhelonkin A. Yu., Ryabova N. V., et al. Influence of geomagnetic disturbances on the ionospheric total electron content // Vestnik of Mari State Technical University. Series: Radio Engineering and Infocommunication Systems. — 2011. — Vol. 1, no. 11. — P. 24–30. — (In Russian).

Karatay S., Arikan F. and Pirti A. Spatio-temporal evaluation of ionospheric disturbances before, during and after earthquakes using differential rate of TEC (DROT) from GPS measurements // Environmental Earth Sciences. — 2025. — Vol. 84, no. 8. — https://doi.org/10.1007/s12665-025-12216-1

Ke F., Wang Y., Wang X., et al. Statistical analysis of seismo-ionospheric anomalies related to Ms>5.0 earthquakes in China by GPS TEC // Journal of Seismology. — 2016. — Vol. 20, no. 1. — P. 137–149. — https://doi.org/10.1007/s10950-015-9516-x

Kelley M. C., Swartz W. E. and Heki K. Apparent ionospheric total electron content variations prior to major earthquakes due to electric fields created by tectonic stresses // Journal of Geophysical Research: Space Physics. — 2017. — Vol. 122, no. 6. — P. 6689–6695. — https://doi.org/10.1002/2016ja023601

Kuo C. L., Huba J. D., Joyce G., et al. Ionosphere plasma bubbles and density variations induced by pre-earthquake rock currents and associated surface charges // Journal of Geophysical Research: Space Physics. — 2011. — Vol. 116, A10. — https://doi.org/10.1029/2011ja016628

Kuo C. L., Lee L. C. and Huba J. D. An improved coupling model for the lithosphere-atmosphere-ionosphere system // Journal of Geophysical Research: Space Physics. — 2014. — Vol. 119, no. 4. — P. 3189–3205. — https://doi.org/10.1002/2013ja019392

Kupovykh G. V. Electric volumetric charge in the surface layer // Izvestiya Taganrog State Radio Technology University. — 1998. — 3(9). — P. 134. — (In Russian).

Levin B. R. Theoretical foundations of statistical radio engineering. — Moscow : Radio i svyaz, 1989. — 653 p. — (In Russian).

Liperovskaya E. V., Parrot M., Bogdanov V. V., et al. On variations of foF2 and F-spread before strong earthquakes in Japan // Natural Hazards and Earth System Sciences. — 2006. — Vol. 6, no. 5. — P. 735–739. — https://doi.org/10.5194/nhess-6-735-2006

Liu J. Y., Le H., Chen Y. I., et al. Observations and simulations of seismoionospheric GPS total electron content anomalies before the 12 January 2010 M7 Haiti earthquake // Journal of Geophysical Research: Space Physics. — 2011. — Vol. 116, A4. — https://doi.org/10.1029/2010ja015704

Liu W. and Xu L. Statistical analysis of ionospheric TEC anomalies before global M w ≥ 7.0 earthquakes using data of CODE GIM // Journal of Seismology. — 2016. — Vol. 21, no. 4. — P. 759–775. — https://doi.org/10.1007/s10950-016-9634-0

Mandrikova O. and Fetisova N. Modeling and analysis of ionospheric parameters based on multicomponent model // Journal of Atmospheric and Solar-Terrestrial Physics. — 2020. — Vol. 208. — P. 105399. — https://doi.org/10.1016/j.jastp.2020.105399

Mandrikova O., Fetisova N. and Polozov Y. Hybrid Model for Time Series of Complex Structure with ARIMA Components // Mathematics. — 2021. — Vol. 9, no. 10. — P. 1122. — https://doi.org/10.3390/math9101122

Mandrikova O. V. and Fetisova N. V. Analysis of Ionospheric Parameter Dynamics During Increased Geomagnetic Activity and Strong Earthquakes in Kamchatka // Problems of Geocosmos-2024. — Cham : Springer Nature Switzerland, 2026. — P. 605–619. — https://doi.org/10.1007/978-3-031-92928-1_45

Mandrikova O. V., Glushkova N. V. and Zhivet'iev I. V. Modeling and analysis of ionospheric parameters by a combination of wavelet transform and autoregression models // Geomagnetism and Aeronomy. — 2014. — Vol. 54, no. 5. — P. 593–600. — https://doi.org/10.1134/s0016793214050107

Mandrikova O. V. and Polozov Yu. A. Criteria of a choice wavelet-function in problems of approximation of natural time numbers difficult structure // Information Technologies. — 2012. — No. 1. — P. 31–36. — (In Russian).

Maruyama T., Tsugawa T., Kato H., et al. Ionospheric multiple stratifications and irregularities induced by the 2011 off the Pacific coast of Tohoku Earthquake // Earth, Planets and Space. — 2011. — Vol. 63, no. 7. — P. 869–873. — https://doi.org/10.5047/eps.2011.06.008

Namgaladze A. A., Klimenko M. V., Klimenko V. V., et al. Physical mechanism and mathematical modeling of earthquake ionospheric precursors registered in total electron content // Geomagnetism and Aeronomy. — 2009. — Vol. 49, no. 2. — P. 252–262. — https://doi.org/10.1134/s0016793209020169

Perevalova N. P., Edemsky I. K., Timofeeva O. V., et al. Dynamics of disturbance level of total electron content at high and middle latitudes according to GPS data // Solnechno-Zemnaya Fizika. — 2016. — Vol. 2, no. 1. — P. 36–43. — https://doi.org/10.12737/13831

Perevalova N. P., Ratovsky K. G., Zherebtsov G. A., et al. Correlation of Short-Period Wave Disturbances of the Peak Electron Density of the F2 Layer and the Total Electron Content in the Ionosphere // Doklady Earth Sciences. — 2023. — Vol. 513, no. 1. — P. 1194–1199. — https://doi.org/10.1134/s1028334x2360192x

Perevalova N. P., Romanova E. B., Katashevtseva D. D., et al. Spatial distribution of total electron content in the Arctic region of Russia from GPS data // Solnechno-Zemnaya Fizika. — 2015. — Vol. 1, no. 4. — P. 40–46. — https://doi.org/10.12737/13832 — (In Russian).

Pestova O., Pestov D., Shishenya A., et al. Electrode layer structure generating under radon-222 transfer across land-atmosphere interface // Proceedings of the XV International Conference on Atmospheric Electricity. ICAE 2014. — Norman : NOAA National Severe Storms Laboratory, 2014. — P. 7–15.

Pulinets S., Ouzounov D., Karelin A., et al. Lithosphere-Atmosphere-Ionosphere-Magnetosphere Coupling-A Concept for Pre-Earthquake Signals Generation // Pre-Earthquake Processes: A Multidisciplinary Approach to Earthquake Prediction Studies. — Hoboken : Wiley, 2018a. — P. 77–98. — https://doi.org/10.1002/9781119156949.ch6

Pulinets S. A. and Boyarchuk K. A. Ionospheric Precursors of Earthquakes. — Berlin : Springer-Verlag, 2004. — 315 p. — https://doi.org/10.1007/b137616

Pulinets S. A., Boyarchuk K. A., Hegai V. V., et al. Conception and model of seismo-ionosphere-magnetosphere coupling // Seismo-Electromagnetics: Lithosphere-Atmosphere-Ionosphere Coupling. — Tokyo : Terrapub, 2002. — P. 353–361.

Pulinets S. A. and Davidenko D. V. The Nocturnal Positive Ionospheric Anomaly of Electron Density as a Short-Term Earthquake Precursor and the Possible Physical Mechanism of Its Formation // Geomagnetism and Aeronomy. — 2018. — Vol. 58, no. 4. — P. 559–570. — https://doi.org/10.1134/s0016793218040126

Pulinets S. A., Davidenko D. V. and Budnikov P. A. Method for Cognitive Identification of Ionospheric Precursors of Earthquakes // Geomagnetism and Aeronomy. — 2021. — Vol. 61, no. 1. — P. 14–24. — https://doi.org/10.1134/s0016793221010126

Pulinets S. A., Davidenko D. V., Ouzounov D. P., et al. Physical bases of the generation of short-term earthquake precursors: A complex model of ionization-induced geophysical processes in the lithosphere-atmosphere-ionosphere-magnetosphere system // Geomagnetism and Aeronomy. — 2015. — Vol. 55, no. 4. — P. 521–538. — https://doi.org/10.1134/s0016793215040131

Pulinets S. A., Davidenko D. V. and Pulinets M. S. Atmosphere-ionosphere coupling induced by volcanoes eruption and dust storms and role of GEC as the agent of geospheres interaction // Advances in Space Research. — 2022a. — Vol. 69, no. 12. — P. 4319–4334. — https://doi.org/10.1016/j.asr.2022.03.031

Pulinets S. A., Hegai V. V., Legen'ka A. D., et al. New Parameter for Analysis of Ionospheric Disturbances and the Search for Ionospheric Precursors of Earthquakes Based on Barbier's Formula // Geomagnetism and Aeronomy. — 2022b. — Vol. 62, no. 3. — P. 255–262. — https://doi.org/10.1134/s001679322203015x

Pulinets S. A., Legen'ka A. D., Hegai V. V., et al. Ionosphere disturbances preceding earthquakes according to the data of ground based station of vertical ionospheric sounding Wakkanai // Geomagnetism and Aeronomy. — 2018b. — Vol. 58, no. 5. — P. 686–692. — https://doi.org/10.1134/s0016793218050110

Pulinets S. A. and Legenka A. D. First simultaneous observations of the topside density variations and VLF emissions before the Irpinia earthquake, 23 November, 1980-2000 // Magnetically Conjugate Regions, International Workshop on Seismo-Electromagnetic of NASDA. Abstracts. — Japan : University of Electro-Communications Publ, 1997. — P. 56–59.

Rodkin M. V. and Liperovskaya E. V. On the difference in physical mechanisms of earthquakes at different depths and their ionospheric response // Izvestiya, Physics of the Solid Earth. — 2023. — Vol. 59, no. 3. — P. 377–390. — https://doi.org/10.1134/s1069351323030114

Romanovskaya Yu. V. and Namgaladze A. A. Ionospheric earthquake precursors: Analysis of total electron content measurements before strong seismic events of the year 2005 // Vestnik MGTU. — 2014. — Vol. 17, no. 2. — P. 403–410. — (In Russian).

Ryabova S. A. and Shalimov S. L. On the Geomagnetic and Ionospheric Variations after the 2023 Strong Eruption of the Shiveluch Volcano // Izvestiya, Physics of the Solid Earth. — 2024. — Vol. 60, no. 4. — P. 612–621. — https://doi.org/10.1134/s1069351324040013

Smirnova E. V. and Smirnov V. M. Total electron content fluctuations of the Earth ionosphere during a maximum and minimum of a solar cycle according to GPS/GLONASS systems // Sovremennye problemy distantsionnogo zondirovaniya Zemli iz kosmosa. — 2013. — Vol. 10, no. 2. — P. 234–240. — (In Russian).

Tachema A. Identifying pre-seismic ionospheric disturbances using space geodesy: A case study of the 2011 Lorca earthquake (Mw 5.1), Spain // Earth Science Informatics. — 2024. — Vol. 17, no. 3. — P. 2055–2071. — https://doi.org/10.1007/s12145-024-01272-z

Taurenis D. A., Barabash N. S. and Ryakhovskiy I. A. TEC dynamics during X-class solar flares // Dynamic Processes in Geospheres. — 2022. — Vol. 14, no. 1. — P. 110–117. — https://doi.org/10.26006/22228535_2022_14_1_110 — (In Russian).

Tsagouri I. Space Weather Effects on the Earth's Upper Atmosphere: Short Report on Ionospheric Storm Effects at Middle Latitudes // Atmosphere. — 2022. — Vol. 13, no. 2. — P. 346. — https://doi.org/10.3390/atmos13020346

Voeykov S. V., Berngardt O. I. and Shestakov N. V. Use of the index of TEC vertical variation disturbance in studying ionospheric effects of the Chelyabinsk meteorite // Geomagnetism and Aeronomy. — 2016. — Vol. 56, no. 2. — P. 219–228. — https://doi.org/10.1134/s0016793216020122

Yasyukevich Y. V., Mylnikova A. A., Kunitsyn V. E., et al. Influence of GPS/GLONASS differential code biases on the determination accuracy of the absolute total electron content in the ionosphere // Geomagnetism and Aeronomy. — 2015a. — Vol. 55, no. 6. — P. 763–769. — https://doi.org/10.1134/s001679321506016x

Yasyukevich Y. V., Mylnikova A. A. and Polyakova A. S. Estimating the total electron content absolute value from the GPS/GLONASS data // Results in Physics. — 2015b. — Vol. 5. — P. 32–33. — https://doi.org/10.1016/j.rinp.2014.12.006

Zakharchenkova I. E., Cherniak Yu. V. and Shagimuratov I. I. Use of signals of global navigational systems GPS/GLONASS for monitoring of the seismo-ionospheric effects // Modern problems of remote sensing of the Earth from space. — 2012. — Vol. 9, no. 3. — P. 156–163. — (In Russian).

Zhang X., Shen X., Parrot M., et al. Phenomena of electrostatic perturbations before strong earthquakes (2005-2010) observed on DEMETER // Natural Hazards and Earth System Sciences. — 2012. — Vol. 12, no. 1. — P. 75–83. — https://doi.org/10.5194/nhess-12-75-2012

Zhang X., Shen X., Zhao S., et al. The characteristics of quasistatic electric field perturbations observed by DEMETER satellite before large earthquakes // Journal of Asian Earth Sciences. — 2014. — Vol. 79. — P. 42–52. — https://doi.org/10.1016/j.jseaes.2013.08.026

Zherebtsov G. A., Shi J., Perevalova N. P., et al. Ionospheric disturbances in East-Asian region. — Moscow : GEOS, 2021. — 340 p. — https://doi.org/10.34756/geos.2021.16.37867 — (In Russian).